The Hilltop Review

Volume 4
Issue 2 *Spring*

Article 9

April 2011

Modeling of a Photonic Crystal Waveguide Modes with the FDTD Method

Buddhi Rai
Western Michigan University

MODELING OF A PHOTONIC CRYSTAL WAVEGUIDE MODES WITH THE FDTD METHOD

By Buddhi Rai
Department of Physics
buddhi.m.rai@wmich.edu

The electromagnetic modes are investigated using a simple 1D implementation of the FDTD numerical algorithm to a model of 1D photonic crystal. The fields E_z and H_y are simulated along the $\hat{x}$ -axis, the propagation direction. Source implementation and the effects of various boundary conditions such as ABC, Mur on TF-SF fields are investigated. Of particular focus in this paper is, for example, on investigating the guided and/or radiation modes at a stop band frequency of the photonic crystal formed of linear and Kerr nonlinear media. Such structures exhibit interesting transmission and reflection properties that make them suitable for optical devices with frequency/ wavelength tunable characteristics.

I. INTRODUCTION

The simulation studies of electromagnetic modes in a photonic crystal have attracted a great deal of interest both practically and scientifically not only because of their potential applications in the field of photonics but also from the point of view of fundamental understanding [1–10]. One focus of particular recent interest has been on the modeling of a waveguide mode arising from nonlinear photonic crystal [11–16]. These types of systems have potential applications in switching and multiplexing designs which may be of importance in routing, uploading, and downloading information carried in optical networks. In this paper our interest will be in guided modes in the simplest case of 1D photonic crystal (layered structure) with a nonlinearity, which is treated and compared with results of the scattering of the modes in the linear limit of the media. The arbitrary layered media, also known as 1D photonic crystal, denotes the structure represented by a number of dielectric layers with arbitrary values of thickness and permittivity [10]. This structure is periodic in one direction and uniform in other two directions.

A wide range of simulation techniques including the plane wave expansion (PWE) and finite-difference time-domain (FDTD) have been developed and utilized for investigating of the scattering and guidance properties of electromagnetic modes in complex photonic crystal structure [12-19]. However, the FDTD method will be considered in details in this paper due to its flexibility to treat almost any types of structures. The conventional PWE method,

although very intuitive and popularly employed in photonic crystal research, suffers from poor convergence and inapplicable to find field distribution in complicated structure or investigate dynamic characteristics. The transfer matrix, finite element, and beam propagation also have been utilized recently. The transfer matrix method can be applied to any periodic structures and many excellent calculations have been performed.

Our particular interest in FDTD method derives from recent research in photonic crystal devices modeling. This method is one of the most advanced methods today particularly for computing the field distribution inside the photonic crystal structures with non-uniform dielectric constant distribution. This is a computationally efficient and stable approach to modeling electromagnetic interactions with arbitrary structures of photonic crystal consisting of various material properties of interest and has been extensively used for predicting behavior of electromagnetic wave scattering and radiation for a variety of practical problems. Some of these works have been conducted by John D. Joannopoulos, J.B. Pendry, Y. Kivshar including others [17–20].

The FDTD technique is based on the numerical time-integration of Maxwell's curl equations. In this technique the computational space is replaced by a discrete set of nodes where finite differences to the spatial and temporal derivatives of the electromagnetic fields of the problem are used as approximations. The numerical approximations allow to setting a system of algebraic equations which are solved sequentially starting from initial and boundary conditions [21, 22]. In this paper, a FDTD code added with the Mur and TF-SF boundary has been developed and validated by performing the initial test on a slab waveguide. The nonlinear media considered in all the simulations reported here are composed of Kerr-type dielectric material with an instantaneous nonlinear response. The nonlinear part of the FDTD code presented in this paper has been developed in the spirit of the work published in [17, 18, 20, 23], and is used to investigate nonlinear periodic media comprising the 1D photonic crystal.

II. FORMULATION

For simplicity, a 1D problem with electric and magnetic field components E_z and H_y propagating in the $\hat{x}$-direction in a homogeneous medium is considered. The propagation has no variations in the $\hat{y}$ and $\hat{z}$ directions, i.e. $\partial/\partial y = \partial/\partial z = 0, \quad \partial/\partial x \neq 0$. Using Fig. 1 as a guide for discretization in space (Yee lattice) and time (leapfrog algorithm, detailed in [21, 22]), Maxwell's curl equations to be implemented in the FDTD form are

$$\nabla \times \vec{H} = \frac{\partial \vec{D}}{\partial t} \quad \Rightarrow \quad E_z^{n+1}(i) = E_z^n(i) + \frac{\Delta t}{\varepsilon} \nabla_x \times \vec{H}_y^{n+\frac{1}{2}} \tag{II.1a}$$

and

$$\nabla \times \vec{E} = \frac{\partial \vec{B}}{\partial t} \quad \Rightarrow \quad H_y^{n+\frac{1}{2}}(i+\tfrac{1}{2}) = H_y^{n+\frac{1}{2}}(i-\tfrac{1}{2}) + \frac{\Delta t}{\mu} \nabla_x \times \vec{E}_z^n \tag{II.1b}$$

which propagate in time steps. The integer i represents the spatial index with $x = i\Delta x$, and the n represents the time step with $t = n\Delta t$ in the FDTD. The $\vec{D} = \varepsilon_0 \varepsilon_r \vec{E}$ and $\vec{B} = \mu_0 \mu_r \vec{H}$, where ε_r and μ_r, respectively, are relative permittivity and permeability of the medium with $\mu_r = 1$ unless stated a different value. The ε_0 and μ_0 are permittivity and permeability of the free space. The $\partial/\partial x$ operates on the fields at the rate of spatial offset Δx on each temporal offset Δt.

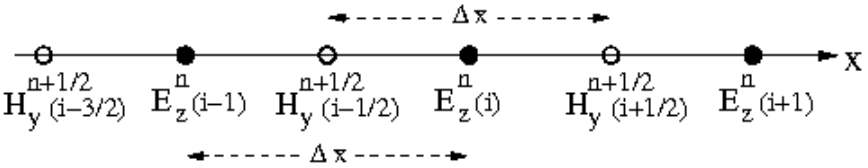

Fig. 1: A typical 1D FDTD space chart of the Yee algorithm showing spatial offset between the electric and magnetic fields, E_z components symbolized as closed circles and H_y components as open circles on the $\hat{x}$ -axis (line of computational domain). The direction of Poynting vector is along the positive *x*-axis.

In order to consider Kerr-type nonlinearity in the medium the permittivity (dielectric constant) shown in the relation $\vec{D} = \varepsilon_0 \varepsilon_r^* \vec{E}$ is simply modeled analytically in terms of electric field intensity described by

$$\varepsilon_r^* = \varepsilon_r + \underbrace{\alpha \chi^{(3)} \mid E \mid^2}_{Kerr} \tag{II.2}$$

where ε_r is the linear part of the nonlinear dielectric constant of the nonlinear medium, α is a constant which dictates the strength of the Kerr nonlinearity, $\chi^{(3)} \approx \chi_0^{(3)}$ (assuming the instantaneous response-model) is the third-order nonlinear dielectric constant of the medium and in this relationship $\chi_0^{(3)}$ has units of m^2/V^2, where *E* is the electric field. The nonlinear dielectric gives rise to a polarization current term in the formulation [23–25]. At that, evaluating each term of Eq. (II.1a), including the Kerr polarization current, and solving for $E_z^{n+1}(i)$, we get the electric field update equation,

$$E_z^{n+1} = \gamma\left(1-5\beta(E_z^{n-1})^2 - 2\beta E_z^{n-1}E_z^n\right)E_z^n - 2\beta\gamma\left(E_z^{n-1}\right)^3 + \gamma\frac{\Delta t}{\varepsilon}\nabla_x \times \vec{H}_y^{n+\frac{1}{2}} \tag{II.3}$$

where $\varepsilon = \varepsilon_0\varepsilon_r$, $\beta = 3\alpha\chi_0^{(3)}/\varepsilon$, and $\gamma = \left(1+\beta(E_z^{n-1})^2\right)^{-1}$. Notice that for zero nonlinear constant, $\chi_0^{(3)} = 0$, the Eq. (II.3) reduces to Eq. (II.1a) which is expected in our treatment.

The updating process starts with the calculation of the new values of the magnetic field component on all the grid points of the computational domain using Eq. (II.1b). By means of the values obtained, the new values of the electric field component are computed in the same way using Eq. (II.3). This approach avoids the necessity of updating the values of the dielectric material of the simulated device, arising due to the nonlinear effects caused by the applied electromagnetic field, because the nonlinear effects are directly applied in the electric field component, E_z, through the computation of Eq. (II.3). Here, the value of E_z from the previous time step is used to calculate the value of E_z in the subsequent time step.

III. NUMERICAL RESULTS

To validate the numerical method developed for the purpose of this paper, a simple case, for example, a slab waveguide, shown in Fig. 2, is considered. This waveguide is composed of a lossless linear dielectric material with dielectric constant $\varepsilon_r = 9$, but this slab is also treated as a nonlinear waveguide comprising the linear dielectric material core with the same linear

dielectric constant, followed by a Kerr dielectric material with nonlinear part of the nonlinear dielectric constant as shown in Eq. (II.2), which is the field intensity dependent in Kerr-type nonlinearity. The structure was excited using a modulated Gaussian pulse (continuous wave) with the shape of the fundamental TE_0 mode profile:

$$E_{z0}(x_0,t) = E_0(x_0)\ \exp\left(-(t-t_c)^2/t_w^2\right)\ \cos\left(2\pi\ f_0\ t\right) \tag{III.1}$$

where $f_0 = 1\times10^{10}\,Hz$ is the modulation frequency, and $E_0(x_0)$ is the fundamental TE_0 mode profile. The excitation only propagates in one direction (positive $\hat{x}$-axis) due to the implementation of TF-SF boundary condition [22].

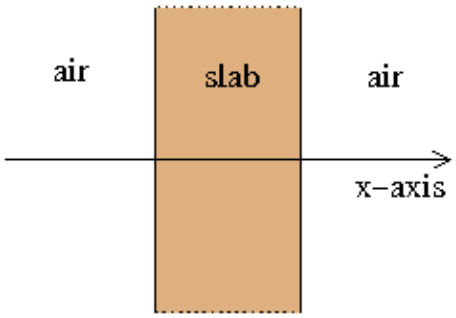

Fig. 2: Schematic diagram of a slab waveguide.

In addition, a differential equation based absorbing boundary condition (ABC), e.g. Mur second order ABC, is implemented to terminate the grid at the boundary ends [22, 26]. Although the Mur ABC is not considered state-of-the-art, it provides a relatively simple way to terminate the grid that is more than adequate in our treatment.

We considered two cases to make sure the FDTD code written for computing the field distribution inside and outside of the layered structure. An example of such a computed field inside the structure containing one layer with dielectric constant $\varepsilon_r = 9$ surrounded by air ($\varepsilon_r = 1$) is shown in Fig. 3 where the inset shows a sequence of the incident pulse with time in free-space alone. In the first case, assuming there is no slab present in Fig. 2, the entire computational space is filled with free space. In this the Gaussian pulse propagates in space

(from left to right) and time (leapfrog method) as shown in the inset. Here, a great deal of utility of waterfall plot is used to display the first 18 snapshots of the electric field in a single image where each snapshot is offset slightly from the next, which is a typical way to ascertain what is happening in the FDTD simulation. In the second case, the dielectric slab is present as described in Fig. 2 above. The slab region is assigned starting at constant, $\varepsilon_r = 9$. The inset shows the electric field distribution when the entire computational domain is filled with free space.

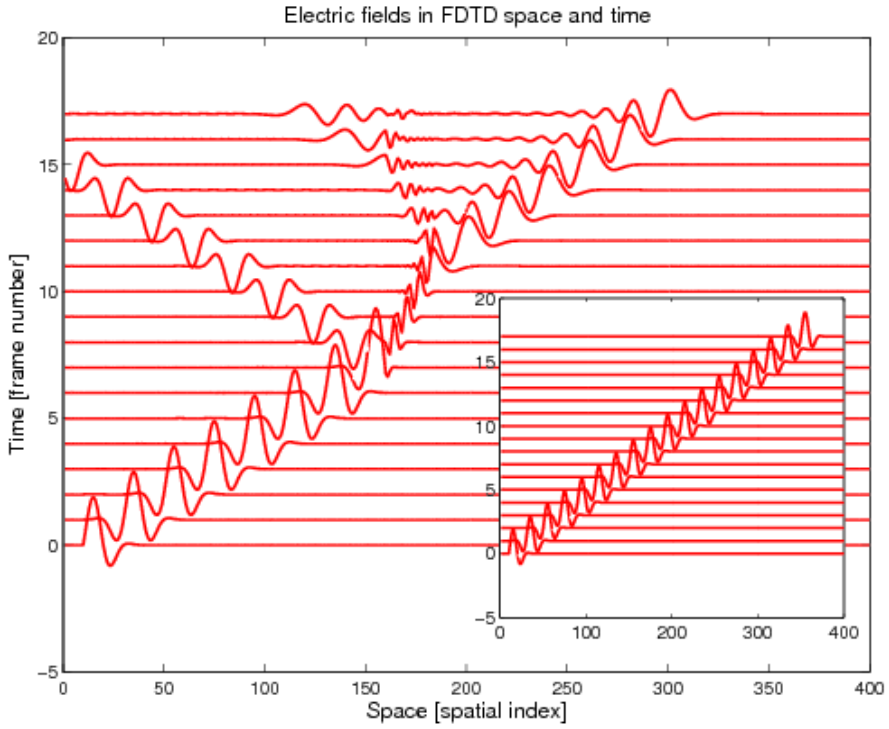

Fig. 3: Waterfall plot of the electric field distribution in a computational domain which has a slab waveguide region (starting at node 150 and ending at node 175) with linear dielectric

Once the field encounters the first interface at node 150, a reflected field (as can be seen just above the frame number 7) is created which is negative and appears to have about half the magnitude of incident pulse. Notice that the peak of the incident field spans a vertical space corresponding to nearly two frames while the peak of the reflected field spans about one frame. Another reflection (with smaller field intensity than the previous) occurs due to second interface at node 175, which is noticeable above the frame number 12. The transmitted pulse is positive and appears to have half the magnitude of the in-

cident field, which can be seen above the frame number 11 on the right of the slab region.

The transmission and reflection coefficients for the slab computed by using the FDTD time response data (spectrum of the output normalized by the spectrum of the input) are presented in Fig. 4. The fields are observed at the ports in front and behind of the slab. The field recorded in front of the slab contains the reflected field as well as the incident field. Therefore, the incident field is subtracted from this data in order to obtain just the reflected field. As seen in the plot, the exact solution agrees with the FDTD result for the slab with linear dielectric material. There is an increase of nonlinear transmittance from its linear counterpart, which will be explained in the next.

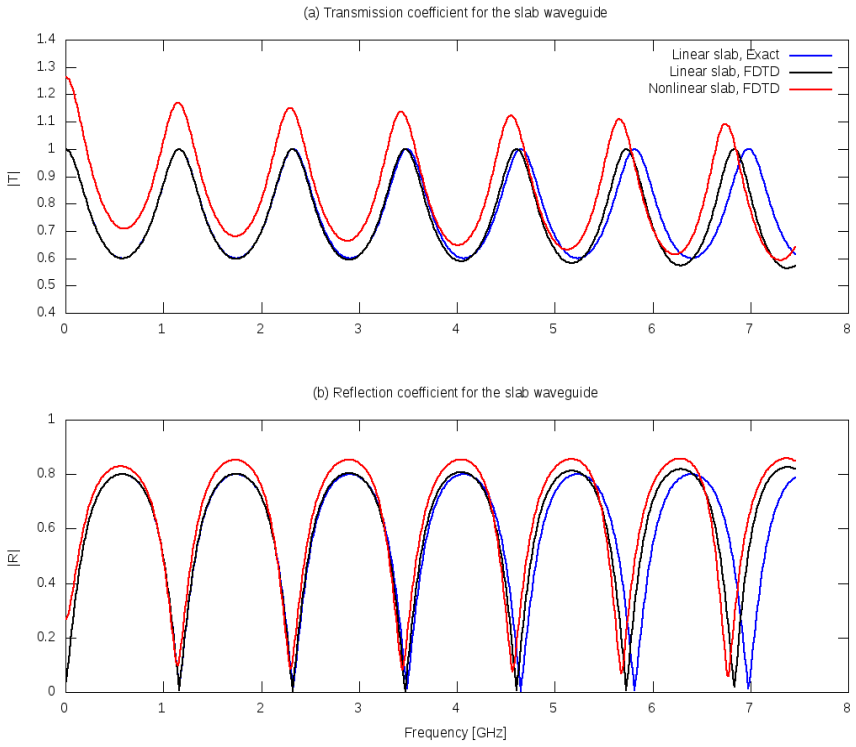

Fig. 4: Transmission and reflection spectra for the slab waveguide.

The transmission and reflection spectra for five lattice layers forming a 1D photonic crystal computed by the time response FDTD method are shown in Fig. 5. The spectra reflect the band structure of the crystal, and they are often used for the design and characterization of real specimens. As is seen in the figure, the transmittance/reflectance is quite different at different frequencies, and because of the periodic lattices, a typical stop band of minimum/

maximum transmittance/reflectance falls at the frequency range 3 to 5 GHz. The magnitude of transmission/reflection coefficient for nonlinear case increases/decreases due to the self-phase modulation (SPM) like effect. The physical system and computation process shown for this result are fairly simple. However, it may have a wide range of applications. Using the FDTD method it is possible to design different passive optical devices high-efficiency reflectors, and anti reflection films, distributed Bragg reflectors for vertical-cavity surface-emitting lasers (VCSEL), wavelength division mux/demux on the basis of fiber Bragg gratings, mirrors of tunable lasers, etc.

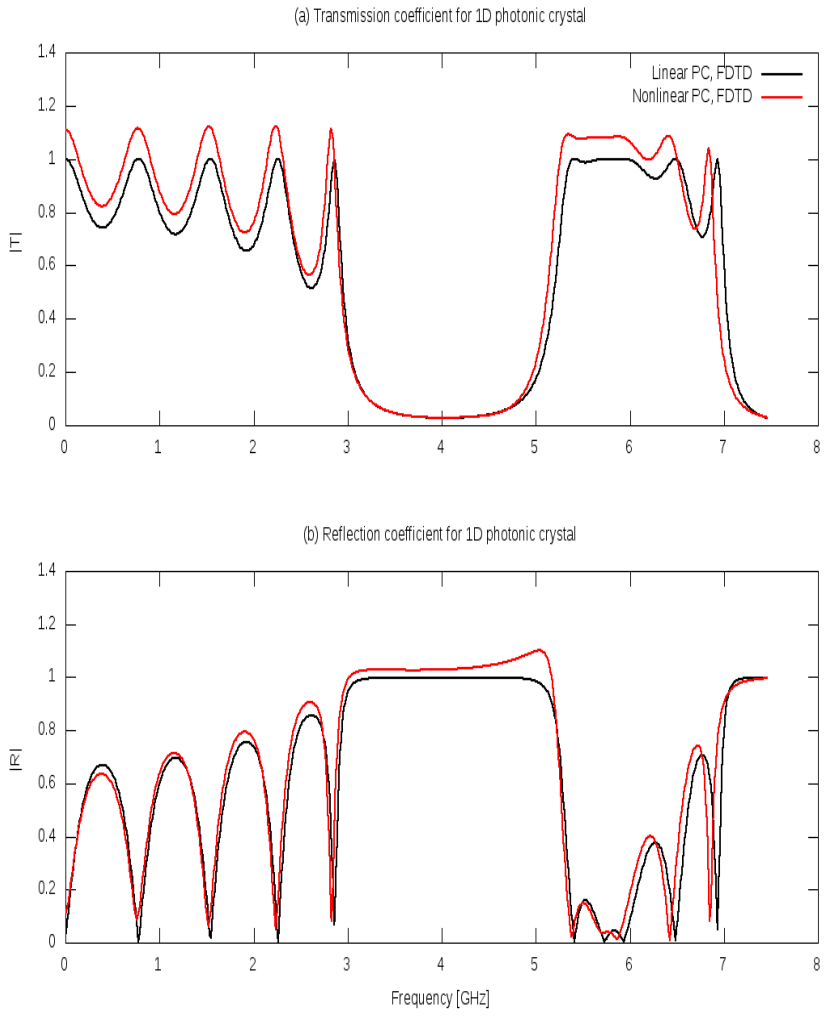

Fig. 5: Transmission and reflection spectra for 1D photonic crystal formed with 5 periods.

IV. CONCLUSIONS

The one dimensional transmission and reflection spectra of linear/ nonlinear periodic media have been successfully simulated with the FDTD method. Using the FDTD code developed to model the slab waveguide, the Kerr-type material with an instantaneous nonlinearity, Bragg reflectors type systems have been investigated. The preliminary results demonstrate the use-fulness of the technique presented in this paper, and thus set the foundation for future computation and design for optical nonlinear devices. The SPM like effect may be applied to switching operations with all-optical components.

References

[1] A. A. Maradudin and A. R. McGurn, *Photonic Band Gaps and Localiza tion* (edited by C. M. Soukoulis, Plenum, New York, 1993).
[2] J. D. Joannopoulos, P. R. Villeneuve, and S. Fan, Nature 386, 143 (1997).
[3] K. Sakoda and H. Shiroma, Phys. Rev. B 56, 4830 (1997).
[4] S. Noda, A. Chutinan, and M. Imada, Nature 407, 608 (2000).
[5] S. F. Mingaleev, Y. S. Kivshar, and R. A. Sammut, Phys. Rev. E 62, 5777 (2000).
[6] K. Sakoda, *Optical Properties of Photonic Crystals* (Sprigner, Berlin, 2001).
[7] J. C. Knight, Nature 424, 847 (2003).
[8] B. Maes, P. Bienstman, and R. Baets, J. Opt. Soc. Am. B 22, 1778 (2005).
[9] J. M. Lourtioz *et al.*, *Photonic Crystals* (Springer, Berlin, 2005).
[10] I. A. Sukhoivanov and I. V. Guryev, *Photonic Crystals* (Springer, Heidelberg, 2009).
[11] P. Tran, Phys. Rev. B 52, 10673 (1995).
[12] F. Raineri, Y. Dumeige, A. Levenson, and X. Letartre, Electronics Letters 38, 1704 (2002).
[13] A. R. McGurn, Chaos 13, 754 (2003).
[14] A. R. McGurn, J. Phys.: Condens. Matter 16, S5243 (2004).
[15] I. S. Maksymov, L. F. Marsal, and J. Pallares, Optical and Quantum Electronics 37, 161 (2005).
[16] S. F. Mingaleev, A. E. Miroshnichenko, Y. S. Kivshar, and K. Busch, Phys. Rev. E 74, 046603 (2006).
[17] R. M. Joseph and A. Taflove, IEEE Transactions on Antennas and Propagation 45, 364 (1997).
[18] T. Hruskovec and Z. Chen, Microwave and Optical Technology Letters 21, 165 (1999).
[19] M. Soljacic, M. Ibanescu, S. G. Johnson, Y. Fink, and J. D. Joannopoulos, Phys. Rev. E 66, 055601(R) (2002).

[20] H.-H. Lee, K.-M. Chae, S.-Y. Yim, and S.-H. Park, Optics Express 12, 2603 (2004).
[21] K. S. Yee, IEEE Trans. Antennas Propagat. 14, 302 (1966).
[22] A. Taflove and S. C. Hagness, *Computational Electrodynamics*, Third ed. (Artech House, Inc., Norwood, MA, 2005).
[23] D. M. Sullivan, IEEE Transactions on microwave theory and techniques 43, 676 (March, 1995).
[24] R. W. Ziolkowski and J. B. Judkins, Radio Science 28, 901 (1993).
[25] J. Li, J. Dai, and P. Wan, Int J Infrared Milli Waves 28, 10111024 (2007).
[26] J. B. Schneider, Understanding the finite-difference time-domain method, www.eecs.wsu.edu/~schneidj/ufdtd, 2010.
[20] H.-H. Lee, K.-M. Chae, S.-Y. Yim, and S.-H. Park, Optics Express 12, 2603 (2004).
[21] K. S. Yee, IEEE Trans. Antennas Propagat. 14, 302 (1966).
[22] A. Taflove and S. C. Hagness, *Computational Electrodynamics*, Third ed. (Artech House, Inc., Norwood, MA, 2005).
[23] D. M. Sullivan, IEEE Transactions on microwave theory and techniques 43, 676 (March, 1995).
[24] R. W. Ziolkowski and J. B. Judkins, Radio Science 28, 901 (1993).
[25] J. Li, J. Dai, and P. Wan, Int J Infrared Milli Waves 28, 10111024 (2007).
[26] J. B. Schneider, Understanding the finite-difference time-domain method, www.eecs.wsu.edu/~schneidj/ufdtd, 2010.